Performance Study on Brackish Water Desalination Efficiency Based on a Novel Coupled Electrodialysis–Reverse Osmosis (EDRO) System

Caixia Fu [1], Fujun Li [2,*], Hui Li [3] and Xuenong Yi [1]

[1] School of Environment and Architecture, University of Shanghai for Science and Technology, Shanghai 200093, China; 15921012381@163.com (C.F.); jackyixn@163.com (X.Y.)
[2] Rizhao Architectural Design and Research Institute Co., Rizhao 276800, China
[3] The Chemours Chemical (Shanghai) Co., Ltd., Shanghai 201204, China; sara.li@chemours.com
[*] Correspondence: lfj20200640@163.com

Abstract: Reverse osmosis (RO) is a commonly used desalination technology, but due to high requirements concerning the quality of the feed water, there still exists permeate flux related to the operating conditions, and the solute removal rate is low. Electric fields have a facilitating effect on RO desalination performance. Previous studies have focused on investigating the combination of RO and electrodialysis (ED) processes separately, without directly exploiting their interactions. To address this issue, this study proposes a novel coupling device that combines both RO and ED technologies in a single unit and investigates their mutual enhancement effects on brackish water desalination. The results show that the coupled EDRO system can mutually enhance the performance of RO and ED processes. The permeate flux ratio of the RO membrane increased with increasing voltage, reaching a maximum value of 23.7% at a feed concentration of 10,000 mg/L. The solute rejection by the ion-exchange membrane also increased with increasing pressure, reaching a maximum value of 14.95% at the same feed concentration. In addition, the specific energy consumption of the coupled system was also reduced compared to a standalone operation, with maximum reductions of 9.5% and 19.2% for RO and 2.5% and 3.4% for ED at 5000 and 10,000 mg/L feed concentrations, respectively.

Keywords: desalination; electric field; reverse osmosis; ion-exchange membrane; coupling

1. Introduction

With the rapid growth of the global economy, urban populations are increasing, and the demand for water resources is growing exponentially, far exceeding the current water-carrying capacity in various regions [1,2]. Water scarcity poses a severe threat to human survival, constrains economic development, and has become a global strategic issue [3,4]. Seawater, as a primary water resource, can be changed into freshwater through desalination. Finding economically efficient ways to desalinate seawater remains a hot topic of research worldwide.

There are primarily two approaches for desalination: thermal desalination and membrane desalination. Since the year 2000, membrane desalination has gained prominence due to its high efficiency and lower operating costs compared to thermal desalination. Approximately 70% of the world's desalination plants primarily utilize membrane desalination technology, with reverse osmosis (RO) comprising the largest share at 64%, and electrodialysis (ED) technology accounting for 4% due to its high rejection rate [5,6].

RO, the most widely used desalination technology, uses pressure above the osmotic pressure of seawater to separate water molecules from salt ions. The main driving force behind RO is a high-pressure pump [7,8]. RO is not only used for seawater desalination, but also for treating brackish water, with the ability to handle salinity concentrations ranging from hundreds to tens of thousands of milligrams per liter [8]. It has advantages such as a

broad range of applications and high treatment efficiency. However, despite the maturity of RO technology, there are still some challenging issues that limit its widespread adoption. RO requires high-quality feedwater and is susceptible to membrane fouling, which decreases the permeate flux [9,10]. The desalination process also generates concentrated brine, which poses an environmental threat [11]. Furthermore, as the salinity of the feedwater increases, there is a decline in the permeate flux, necessitating higher energy consumption to meet the production demands [12]. These limitations impede further expansion of the RO market, and solutions to these challenges are urgently needed.

ED technology is involved in a process that separates salt and water by applying an electric field [5]. Under normal conditions, ED systems do not require high-pressure pumps for boosting [13–15]. According to simulations, ED has an advantage over RO in terms of energy consumption when treating brackish water up to 5 g/L, with 80% of salt removal achieved with less than 0.6 kWh/m^3 of energy [16]. It offers advantages such as easy operation and maintenance, low pretreatment requirements, and a long lifespan, making it widely applied in brackish water desalination, wastewater treatment, and metal recovery [17–19]. While the energy consumption of RO is lower than ED in seawater desalination applications, ED has lower energy consumption in brackish water applications [20,21]. However, ED is impacted by the resistance of the solution and current density limits, which can lower the current efficiency [22]. Therefore, improving the current efficiency of ED remains a challenge that needs to be addressed.

Based on the characteristics of RO and ED, many researchers have combined the use of these two technologies to enhance desalination efficiency and recovery rates. Generous (2021) proposed a novel brackish water ED–RO process, demonstrating that the integrated ED–RO system outperformed standalone ED or RO systems when the feed solution salinity ranged from 2.5 to 7.8 ppm [23]. Zhang (2021) researched combining ED and RO to treat desulfurization wastewater, with near-zero discharge. The study achieved a significant concentration increase from 78 g/L to 230 g/L, while producing product water with a conductivity of 550 μs/cm [24]. Similarly, Nayar (2019) investigated the integration of RO and ED related to seawater concentration, in the context of salt production. The study revealed the potential for cost reduction ranging from 33% to 70% compared to using standalone ED systems [25]. Moreover, to improve the recovery rate of RO, Walker (2014) used ED to treat the concentrate from a BWRO system (TDS: 7890 mg/L), achieving a high salt removal rate of up to 99%, with a current density of less than 280 A/m^2 [26]. To reduce energy consumption and desalination treatment costs, Gurreri (2022) employed combined electrodialysis and RO processes (ED–RO, RED–RO, ARED–RO) for seawater treatment. The seawater was pretreated using ED and then desalinated using RO, resulting in the combined process achieving maximal production rates and minimal energy consumption [27]. The combination of ED and RO is a promising integrated technology and has attracted much attention [28,29].

However, previous studies on the combination of RO and ED have mostly focused on the integration of individual units in a sequential manner, where each system operates independently. While this approach can enhance desalination efficiency and reduce energy consumption, it does not fully utilize the energy fields of both technologies. Research indicates that the application of an electric field can reduce membrane fouling and improve the permeate flux in RO processes [30–32]. Simultaneously, enhancing the water inlet pressure and flow rate, without damaging ion-exchange membranes, can improve the mass transfer efficiency in ED [33]. To address these issues, building on previous research, a proposed approach involves integrating RO and ED into a single device. In this configuration, the concentration effect of RO can provide a higher solute concentration for ED, thereby increasing the current density. Additionally, the ion migration effect of ED can reduce the osmotic pressure on the outer side of the RO membrane, subsequently lowering the operating pressure. Furthermore, the electric field can positively influence membrane performance, leading to an improved solute rejection rate and permeate flux.

This study is centered on the desalination of brackish water using a newly developed EDRO (electrodialysis–reverse osmosis) coupled unit. The primary aim is to assess the viability of the EDRO coupling device for desalination. Specifically, this study examines variations in the solute removal rate and permeate flux of reverse osmosis membranes, as well as changes in the solute removal rate and the current efficiency of ion-exchange membranes operating under coupling conditions. Furthermore, this study encompasses pertinent economic analyses. Ultimately, the objective of this research is to advance in a new direction in regard to desalination technology.

2. Materials and Methods

2.1. Materials

The RO membrane used in this study was purchased from Changsha Funuo Environmental Protection Technology Co., Ltd., Changsha, China, and the solute rejection rate was 99.7%. The ion-exchange membrane was purchased from Wuxi Hengrui Water Treatment Equipment Co., Ltd., Wuxi, China, with a solute rejection rate of 40%. The polytetrafluoroethylene (PTFE) sheet was purchased from Shandong Taohong Wear-Resistant Materials Co., Ltd., Dezhou, China, and the titanium-coated ruthenium electrode plate was purchased from Shanxi Youchuang Environmental Technology Co., Ltd., Xi'an China. The DC power supply, with a voltage range of 0–50 V, was procured from Jiangsu Ritai Environmental Protection Engineering Co., Ltd., Yancheng, China.

We used analytical grade reagents, including NaCl, HCl, and NaOH, which were purchased from Shanghai Sinopharm Chemical Reagent Co., Ltd., Shanghai, China.

2.2. Test Equipment

The EDRO coupling device used in this research comprises an ED unit and an RO unit. The ED unit comprises two titanium-coated ruthenium electrode plates and five chambers. The RO unit is integrated into the dilute chamber of the ED unit, as depicted in Figure 1. The five chambers in the ED unit are arranged with paired cation-exchange and anion-exchange membranes. The chambers, from left to right, are the electrode chamber, dilute chamber 1, concentrate chamber, dilute chamber 2 (with RO membrane), and electrode chamber.
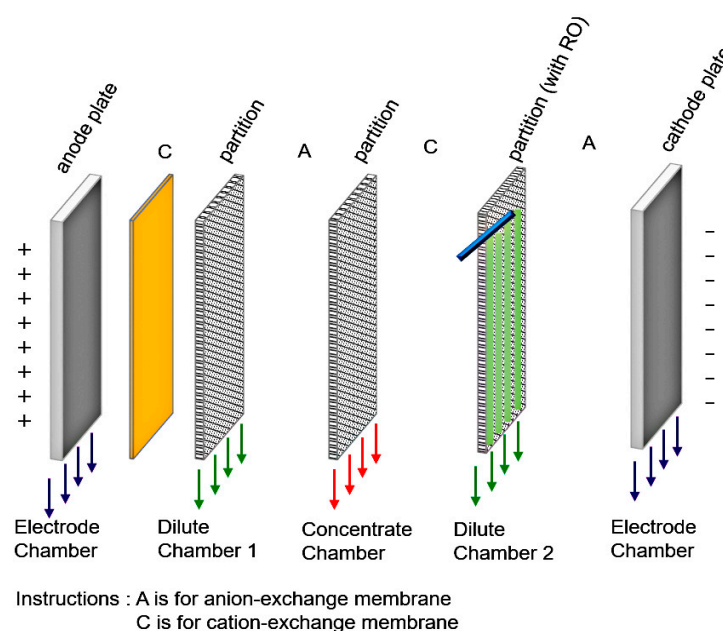

Figure 1. Schematic diagram of EDRO coupling equipment.

The compartment barrier is constructed using a 20 mm thick piece of PTFE material. It features a hollow center filled with a diamond-shaped mesh and is sealed around the edges using 6 mm O-rings. The dimensions of the barrier are 595 × 295 × 20 mm, while

the hollow section measures 378 × 148 mm. The ion-exchange membrane measures 408 × 198 mm, with the effective size being 325 × 140 mm. The electrode plates, coated with titanium–ruthenium, are 325 × 140 mm in size. They are securely fixed within the barrier using waterproof adhesive and sealed with 6 mm O-rings around the edges.

The RO system consists of two homemade RO membranes, a permeate flow net, and a water collection pipe. These components are assembled into a membrane bag form with three sealed sides, and one side is connected to the water collection pipe, as shown in Figure 2b. The permeate flow net is placed between the two membranes to guide the desalinated water passing through them. The water collection pipe has a diameter of 6 mm with surface perforations of 1 mm, which allows it to collect the desalinated water. The homemade RO system has dimensions of 300 mm in length and 96 mm in width. In this setup, the size of the RO system is intentionally kept smaller than the effective size of the compartment to ensure that it does not obstruct the passage of ions through it.
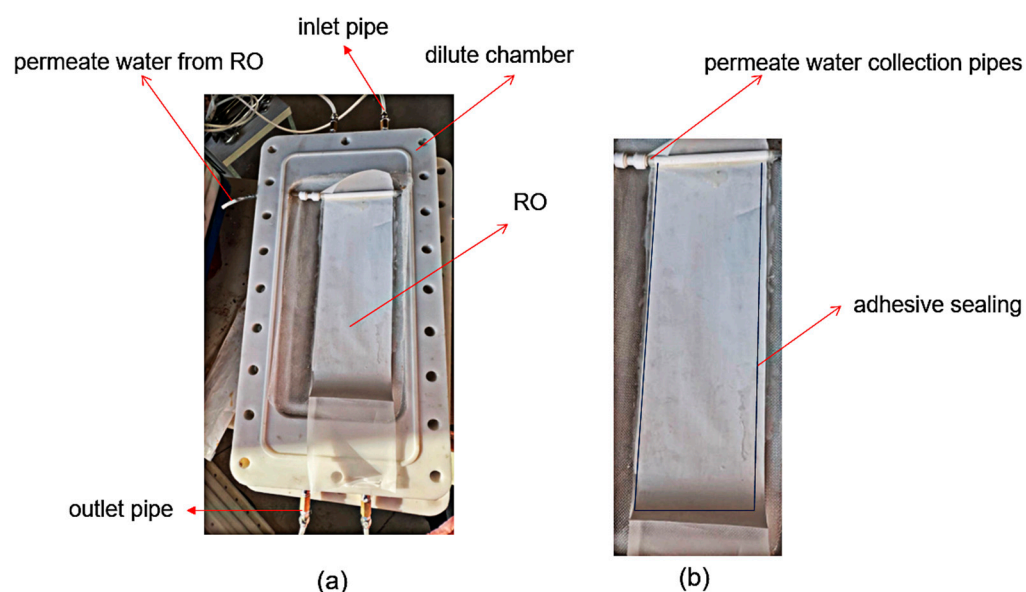

Figure 2. RO and ED coupling diagram: (**a**) chamber with RO, (**b**) developed RO system.

In the EDRO coupled system, each compartment has separate inlet and outlet pipes, with valves for flow and pressure control. To couple the RO with ED, the RO membrane is embedded in the partition layer of dilution chamber 2, and the freshwater outlet pipe in the RO system is situated near the inlet end of the compartment, as shown in Figure 2a. Both the RO and ED systems share the same dilution chamber 2 as the inlet system.

A photo of the EDRO equipment can be found in Figure 3.

Figure 3. A photo of the EDRO equipment.

The EDRO experimental system consists of a feed tank, a high-pressure pump, pressure gauges, flow meters, valves, the main body of the EDRO equipment, and a DC power supply, among others. Both the pressure and the flow rate in the EDRO system are controlled through inlet and outlet valves in each compartment.

When the ED operates independently without internal pressure (which is insufficient for RO operation), the water collection pipe in the RO system does not discharge water, and ions migrate directionally in response to the electric field effect through the ion-exchange membranes for desalination. When the RO system operates independently without an additional electric field, ions do not migrate directionally, and the water in dilution chamber 2 is filtered through the RO membrane due to pressure. The desalinated water flows out through the water collection pipe, while the remaining concentrated water stays in dilution chamber 2 and, eventually, flows out directly through the outlet pipe at the end of dilution chamber 2.

When both ED and RO operate simultaneously, a portion of the water in dilution chamber 2 passes through the RO membrane due to pressure, which is collected by the water collection pipe, and flows out from near the inlet end of the compartment. Meanwhile, the concentrated water remains in dilution chamber 2. Additionally, due to the electric field, the water in dilution chamber 2 undergoes further desalination and, eventually, flows out from the end of dilution chamber 2.

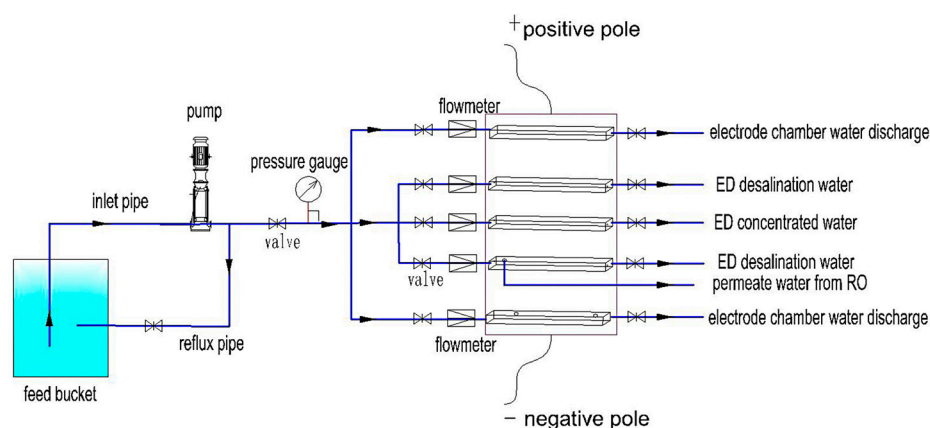A diagram of the test system is shown in Figure 4.

Figure 4. Schematic diagram of the EDRO test system.

2.3. Ion Migration Patterns in EDRO Systems

In an integrated EDRO system, let us illustrate the process of ion migration using the example of a dilution chamber with RO, with the solution being a NaCl solution. Figure 5a demonstrates that, during the simultaneous operation of ED and RO, ions migrate directionally in the dilute chamber under the influence of an electric field. The anion-exchange membrane selectively allows Cl^- ions to pass through, while the cation-exchange membrane only permits Na^+ ions, leading to a gradual decrease in the ion concentration within the dilute chamber. Concurrently, as water permeates the RO under pressure, the microporous structure of the membrane effectively hinders the passage of most ions, resulting in the production of permeate water within the RO. This permeate water then flows out through the pipe. Within the remaining dilute chamber, the decreasing presence of water molecules causes a relative increase in the ion concentration, lowering the solution resistance. This phenomenon contributes to the enhancement of the desalination efficiency within ED. The desalination effect of the ED on the RO triggers an increase in the production of permeate water under the same pressure, due to a reduction in the concentration of the main solution.
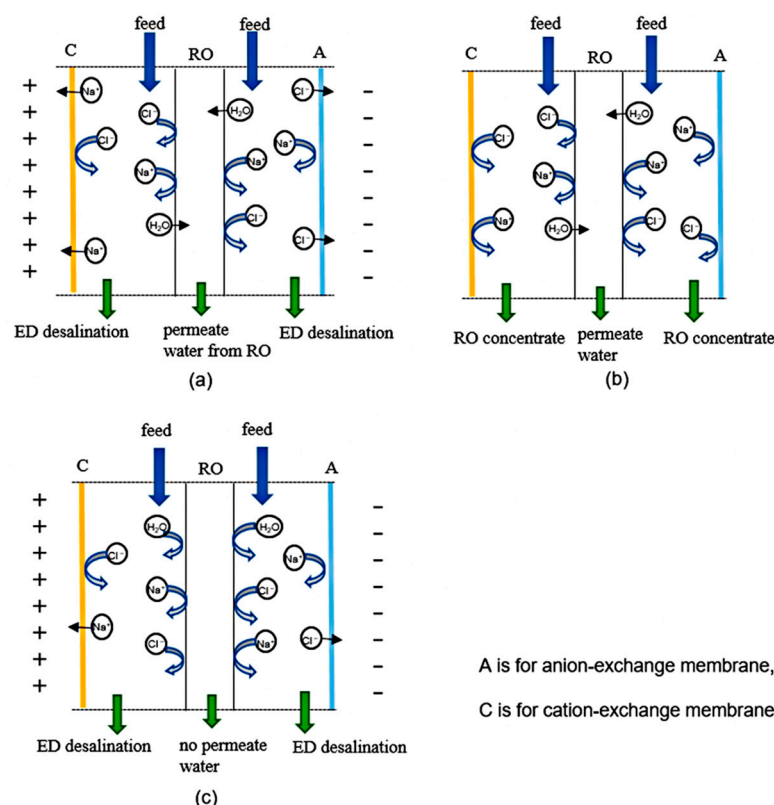
Figure 5. Schematic diagram of the ion migration pattern in the EDRO system: (**a**) ED and RO working simultaneously, (**b**) RO working alone, (**c**) ED working alone.

When RO is the only mechanism at work, ion migration is as shown in Figure 5b: In the absence of an electric field, ED is inactive, preventing ions from passing through the anionic and cationic membranes. As a result, water molecules permeate outward through the RO membrane to form permeate water, while the concentrated water is discharged directly.

In the single ED scenario, anions are selectively allowed to pass through the anion-exchange membrane under the influence of an electric field, while cations are blocked. Similarly, cations pass through the cation-exchange membrane to the exclusion of anions. However, without the presence of pressure, water molecules are unable to pass through the RO, resulting in the absence of osmotic water flow. Consequently, the only end product from the ED process is desalinated water.

2.4. Experimental Design

The experiment is divided into five parts. Firstly, separate experiments are conducted on the RO system and the ion-exchange membrane system in relation to the EDRO coupled equipment to verify whether their desalination patterns align with previous research [34–38]. This is referred to as single-field source testing. In the experiment, artificially prepared feed water is utilized, and the pH of the inlet water is controlled within the range of 7.0 ± 0.35, by adjusting it using HCl and NaOH. The temperature is maintained at $23\,°C \pm 0.5$ with the help of a heating rod or cooling water.

The coupled equipment utilizes the same high-pressure pump. Due to experimental limitations, the feed water in the aqueous chamber, dilute chamber, and concentrate chamber are the same. The total flow rate in the dilute and concentrate chambers is maintained at a constant 1.5 L/h. The inlet water ratio is maintained at 1:1. The pressure in the coupled equipment is controlled using valves in the brine chamber and a drain valve. Each experimental group is initially operated for 30 min and then tested once the system reaches a stable state.

Tables 1–5 outline the pivotal experimental steps for the EDRO system: Table 1 evaluates the RO system tests subjected to a single pressure field; Table 2 analyzes the ion exchange membrane experiments subjected to a single electric field; Tables 3 and 4, respectively, investigate the effect of the coupled state involving an electric field and a pressure field on the desalination performance of RO and ED; Table 5 examines the energy consumption of the EDRO system.

Table 1. RO system tests subject to a single pressure field.

No.	Feed Water Total Dissolved Solids (TDS) (mg/L)	Operating Pressure (MPa)	Sampling Methods
1	3000		Each 1 h period is treated as a separate operational unit. During this time, three parallel samples are consistently collected for analysis. The salt concentration of each sample, as well as the total volume of permeate water within the 1 h duration, are carefully recorded.
2	5000	0.33, 0.60, 0.85, 1.20	
3	8000		
4	10,000		

Table 2. Ion-exchange membrane experiments subject to a single electric field.

No.	Feed Water TDS (mg/L)	Voltage (V)	Sampling Methods
1	3000		Each 1 h period is considered as one operational unit. During this time, three parallel samples are continuously collected to detect the salt concentration in the dilute chamber. Additionally, the operational voltage and current are recorded.
2	5000	10, 15, 20, 25	
3	8000		
4	10,000		

Table 3. RO membrane experiments in the coupled state involving an electric field and pressure field.

No.	Feed Water TDS (mg/L)	Operating Voltage (V)	Operating Pressure (MPa)	Sampling Methods
1	3000		0.33	Each 1 h period is considered as one operational unit. During this time, three parallel samples are continuously collected. The overall experimental duration for each set is 4 h. The TDS value of each sample is recorded, along with the total volume of permeate water for each 1 h interval.
2	5000	10, 15, 20, 25	0.60	
3	8000		0.85	
4	10,000		1.20	

Table 4. Experiments on ion-exchange membranes in the coupled state involving an electric field and pressure field.

No.	Feed Water TDS (mg/L)	Operating Voltage (V)	Operating Pressure (MPa)	Sampling Methods
1	3000		0.33	Each 1 h interval is treated as an operational unit, during which three consecutive parallel samples are taken. The aim is to measure the TDS value, as well as the voltage and current during each sample collection.
2	5000	15	0.60	
3	8000		0.85	
4	10,000		1.20	

Table 5. Energy consumption analysis experiment.

No.	Feed Water TDS (mg/L)	Operating Voltage (V)	Operating Pressure (MPa)	Sampling Methods
1	5000		0, 0.6	The total volume of treated water is 4.5 L and the treatment time is 3 h. Upon completion of the treatment, the amount of permeate water and TDS values produced by the RO system will be recorded, along with the TDS values and current in the dilute chamber of the ED system.
2	10,000	0, 10, 15, 20, 25	0, 1.2	

2.5. Parametric Equation

To evaluate the desalination performance of ion-exchange and RO membranes in EDRO systems, the following parametric indicators were used.

The solute removal rate R represents the membrane's ability to remove solutes and is expressed as follows:

$$R = 1 - \frac{C_d}{C_{in}} \times 100\% \tag{1}$$

where C_d (me/L) represents the concentration of reverse osmosis membrane permeate water or ED membrane desalinated water, while C_{in} (me/L) represents the solute concentration of the feed water.

The permeate flux J (L/m^2·h) represents the volume of water passing through a unit area of the RO membrane in a unit of time. The formula is given as follows:

$$J = \frac{V}{A \times T} \tag{2}$$

where V (L) represents the total volume of water that has passed through the reverse osmosis membrane; A (m^2) is the effective surface area of the RO membrane; T (h) is the operating time.

The current efficiency η is an important indicator for assessing the efficiency of the current utilization in ED processes. It represents the proportion between the input current in the ED system and the theoretical current required for electrolyte transfer. The formula is as follows:

$$\eta = \frac{\frac{Q}{n} C_{in} - C_d \times 96500}{3600 I} \times 100\% \tag{3}$$

where Q (m^3/h) represents the flow rate of the water being treated; n is the number of membrane pairs in the ion-exchange membrane; I (A) is the operating current.

The change in the permeate flux of the RO membrane with and without an electric field is expressed using the permeate flux variation ratio. The formula is as follows:

$$\theta = 1 - \frac{J_o}{J_d} \times 100\% \tag{4}$$

where J_o (L/m^2·h) represents the permeate flux of the RO membrane when both the electric field and pressure field are present, and J_d (L/m^2·h) is the permeate flux without an electric field.

The change in the solute rejection rate of an RO or ion-exchange membrane when both an electric field and pressure field are present, compared to when only a single field is present, is represented using the solute rejection rate variation ratio (τ). The formula is as follows:

$$\tau = 1 - \frac{R_o}{R_d} \times 100\% \tag{5}$$

where R_o represents the solute rejection rate of the RO or ion-exchange membrane when both the electric field and pressure field are present, and R_d represents the solute rejection rate of the membrane when only a single field is present.

2.6. Analytical Methods

During the experiment, the water intake, pressure, current, and voltage of the coupled system were monitored in real-time, using a flow meter, manometer, ammeter, and voltmeter, and the TDS and pH values of the water were measured using a conductivity meter (DDS-307A, Shanghai Yidian Scientific Instrument Co., Ltd., Shanghai, China) and an acidity meter (PHS-25C, Shanghai Yidian Scientific Instrument Co., Ltd., Shanghai, China). To measure the volume of the water produced, a measuring cylinder was used for accurate measurements. Meanwhile, to ensure the accurate dosage of chemicals, we used a one-in-ten-thousand analytical balance (FA124, Shanghai Shunyu Hengping Scientific Instrument Co., Ltd., Shanghai, China) to weigh the chemicals used.

3. Results and Discussion

3.1. Effect of Operating Pressure on Solute Removal and Permeate Flux in RO

Figure 6 illustrates that the solute removal rate of the RO membrane remains relatively stable, exceeding 90%, regardless of the pressure variation at different solution concentrations. However, at a concentration of 10,000 mg/L, the solute removal rate varies between 85% and 95%. This variability can be attributed to the higher concentration of NaCl, where, at low driving pressures, the transfer rate of NaCl outpaces the permeation rate of water, resulting in a reduced amount of water passing through the membrane, subsequently leading to a decrease in the solute removal rate.

Figure 6. Variation in the solute rejection, during RO, at different pressures and concentrations.

Based on Figure 7, it can be observed that the permeate flux concerning the RO membrane increases with the increasing pressure at different solution concentrations. Additionally, lower solution concentrations exhibit higher permeate flux, which is consistent with previous research findings [36]. Previous studies have indicated that the permeate flux is not only influenced by the membrane properties, but is also positively correlated with pressure [12,39]. This is because the permeation of water requires overcoming the osmotic pressure of the solution, and a greater external driving force results in a larger amount of water permeating through the membrane. However, as the solution concentration increases, the osmotic pressure of the solution also increases, leading to a reduction in the amount of water permeating through the membrane at the same pressure.
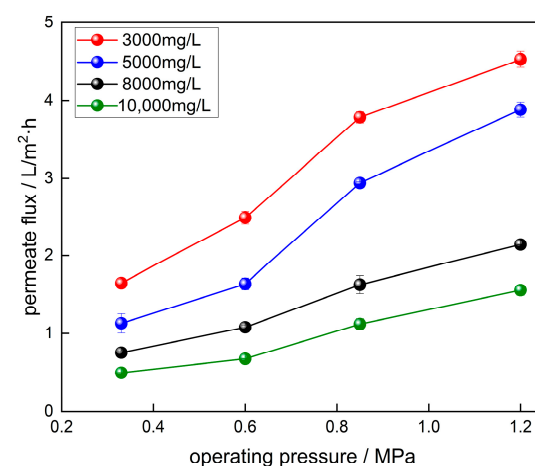

Figure 7. Variation in the permeate flux, concerning the RO membrane, at different pressures and concentrations.

Based on the above experimental results, it can be seen that the desalination performance of the RO membrane in the EDRO coupled unit is consistent with the results in previous studies. This indicates that the RO membrane in the unit is operating effectively.

3.2. Solute Removal and Current Efficiency of Ionic Membranes subject to Different Electric Fields and Concentrations

According to the results shown in Figure 8, it can be observed that for the same solution concentration, the solute removal rate of the ion membrane also increases as the voltage gradually increases. At a voltage of 25 V, the solute removal rates for solutions with concentrations of 3000, 5000, 8000, and 10,000 mg/L, reach their maximum values, which are 29.0%, 34.0%, 40.0%, and 48.0%, respectively. The reason for this phenomenon is that as the incoming salt concentration increases, the concentration difference between the incoming water and the freshwater also increases. As a result, the driving force of the mass transfer caused by the concentration difference increases. In addition, the system resistance decreases as the incoming salt concentration increases, which reduces the mass transfer resistance caused by the potential difference. The combination of these factors improves the total mass transfer rate of the plant. Furthermore, as the voltage increases, the electric field strength also increases, resulting in a greater electric field force acting on the ions. This accelerates the migration speed of the ions, making it easier for them to pass through the membrane and, thus, increasing the desalination efficiency.
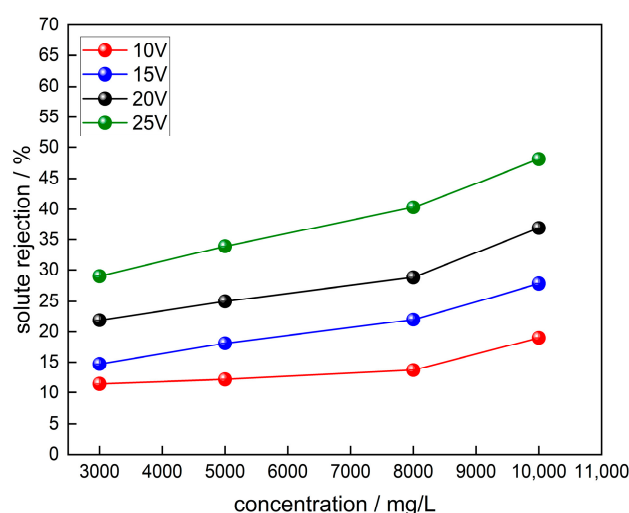

Figure 8. The solute rejection rate of ionic membranes subject to different electric fields.

Figure 9 displays similar current efficiency values for different salt concentrations and voltages, ranging from 80% to 90%. According to Equation (3), the current efficiency is dependent on the solute removal and the current. Within a certain voltage range, as the voltage increases, the electric field driving force strengthens, leading to an increase in ion migration and a higher current efficiency, as observed in the cases of 5000, 8000, and 10,000 mg/L. However, with a further increase in voltage, the current reaches a certain level where a large number of ions migrate from the dilution region to the concentration region. This amplifies the concentration difference and intensifies water diffusion through the concentration gradient, potentially resulting in a decrease in the current efficiency. When treating a salt solution with a concentration of 3000 mg/L, there is a downward trend in the current efficiency. A possible explanation for this is that, with an elevated voltage, the ion migration speed becomes too rapid, and the ions in the boundary layer are not replenished promptly. This also aggravates the concentration polarization, thereby reducing the current efficiency.
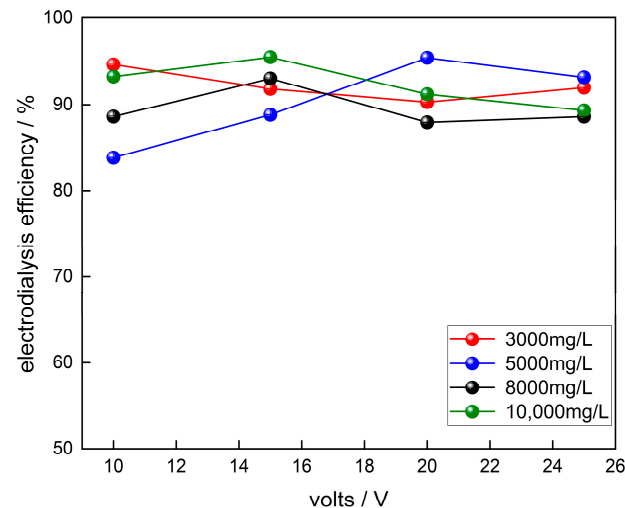
Figure 9. The current efficiency of the ionic membrane subject to different electric fields.

3.3. Effect of RO and Ion Membrane Performance in a Coupled System

3.3.1. Effect of Electric Field on Solute Removal and Permeate Flux in RO

As shown in Figure 10, the electric field enhances the permeate flux of RO, with a higher voltage leading to a greater rate of change in the permeate flux. At a feed water concentration of 3000 mg/L, the minimum rate of change in the permeate flux for the membrane is 4.57% (10 V), while the maximum is 9.91% (25 V). At a salinity of 5000 mg/L, the minimum change in the permeate flux is 5.04% (10 V), and the maximum is 10.5% (25 V). At 8000 mg/L salinity, the permeate flux rate change is 10.44% (10 V), and the maximum change is 21.2% (25 V). For a feed water salinity of 10,000 mg/L, the minimum ratio of change in the osmotic flux is 15.36% (10 V), and the maximum is 23.7% (25 V).
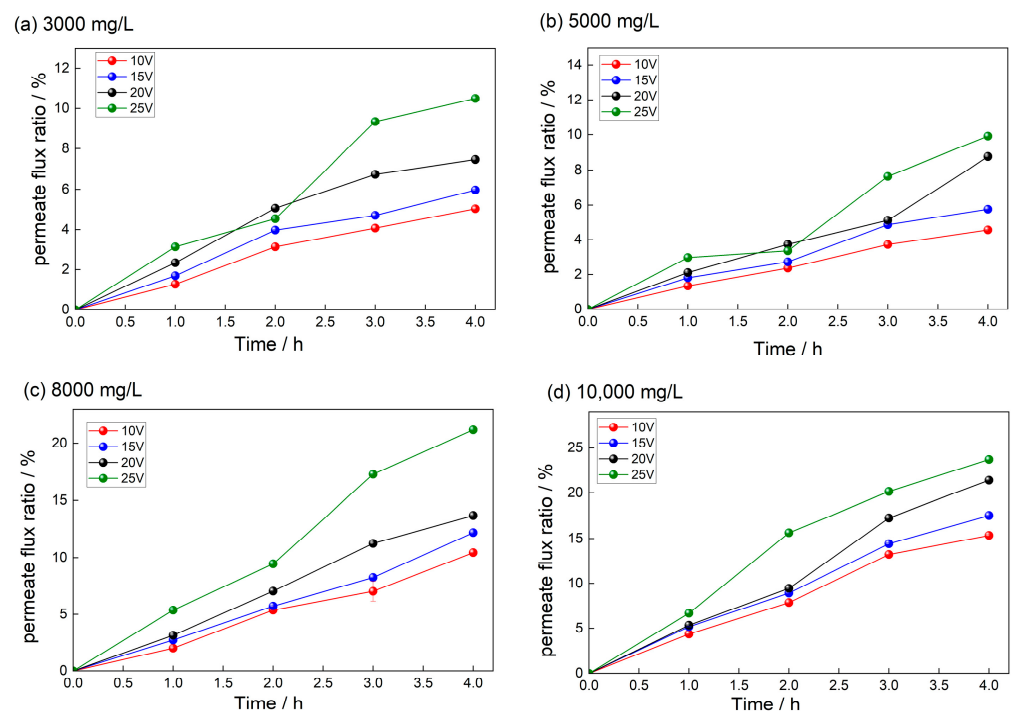

Figure 10. The permeate flux ratio, during RO, subject to varying electric fields.

This phenomenon can be attributed to the fact that the permeate flux is directly proportional to the water production, which increases with the operating pressure. In this experiment, the operating pressure was kept constant, but the external electric field created a region of fresh water and concentrated water on the membrane surface. In the freshwater region, the salt concentration decreases, resulting in a decrease in the required osmotic pressure. Therefore, at a constant inlet pressure, the electric field enhances the permeation drive, leading to an increase in the permeate flux.

Linear regression analysis was performed to investigate the relationship between the permeate flux during RO and voltage. Figure 11 shows that the R^2 values are all greater than 0.9, indicating that there is a strong correlation between the permeate flux and the operating voltage. It is evident from the graph that as the voltage increases, the permeate flux also increases, especially at higher salt concentrations (8000 mg/L and 10,000 mg/L). This is because, at higher feed salt concentrations, ED becomes more efficient, resulting in significant changes in the salt concentration in the desalinated region. As a result, there is a larger osmotic pressure drop, further enhancing the driving force and leading to a greater increase in the permeate flux.
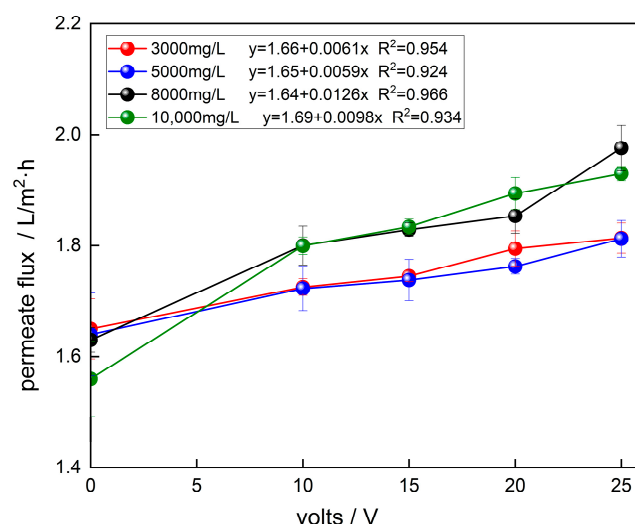

Figure 11. Linear fit of voltage to permeate flux.

Additionally, as water molecules are polar and dielectric, the presence of an electric field accelerates their motion and promotes the disruption of hydrogen bonds and polarization within the water molecules. In the presence of ions in the solution, electrostatic interactions occur between the ions and the local charges of water molecules, resulting in the formation of solvation shells around the ions, known as hydrated ions. Hydrated ions are strongly attracted to electric fields, making them more prone to movement under its influence [40–42]. As the ion concentration in the solution increases, the ion activity becomes more pronounced and the effect of the electric field on water becomes more significant, resulting in greater permeate flux fluctuations.

3.3.2. Effect of Electric Field on Solute Rejection Rate in RO

Figure 12 depicts the variation in the solute removal rate with respect to voltage, for different concentrations, after the EDRO system has been in operation for 4 h. It can be observed from the graph that, at different concentrations, there is little change in the solute removal rate with increasing voltage compared to the condition without an electric field (0 V), showing that the electric field has no significant effect on the solubility of the substance.
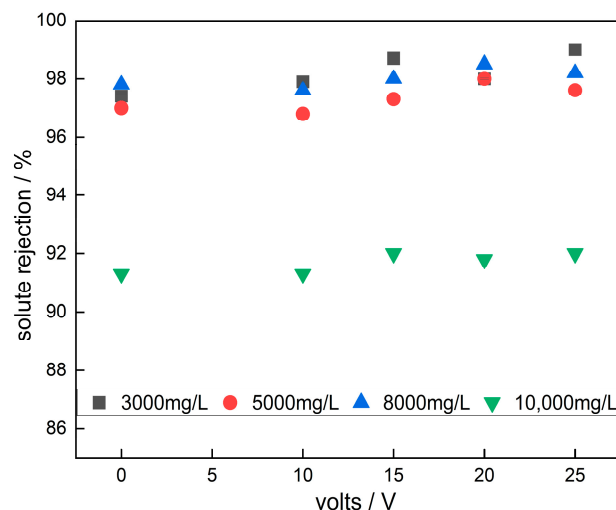
Figure 12. Effect of voltage on solute removal during RO.

3.3.3. Effect of Pressure on Solute Rejection and Current Efficiency of Ionic Membranes

The main focus of this experiment is to investigate the impact of pressure on the desalination performance of ion-exchange membranes in the EDRO system, disregarding the influence of voltage. In the preliminary experiments, it was observed that higher voltages led to more severe dissociation of chloride ions at the electrode. Therefore, a fixed operating voltage of 15 V was chosen for this experiment, with operating pressures set at 0, 0.33, 0.6, 0.85, and 1.2 MPa. This allowed us to examine the variation in the solute rejection rate ratio and the current efficiency of the ion-exchange membrane under different solution concentrations.

Figure 13 shows that pressure has a positive effect on the solute rejection rate of ion-exchange membranes. As the pressure increases, the rate of change in the solute rejection rate also increases, but it does not follow a linear growth pattern. The effect of pressure on the membrane is mainly demonstrated by the RO membrane, which allows water to pass through, resulting in an increase in the salt concentration in the solution and, consequently, increasing the number of ions migrating to the surface of the ion-exchange membrane under the same electric field strength. The increase in solution concentration reduces the resistance of the desalination channel and decreases the mass transfer resistance caused by the potential difference. At the same time, an increase in pressure can also increase the turbulence of the solution, leading to a higher convective mass transfer rate of ions, thereby improving the salt removal efficiency of the ion-exchange membrane.
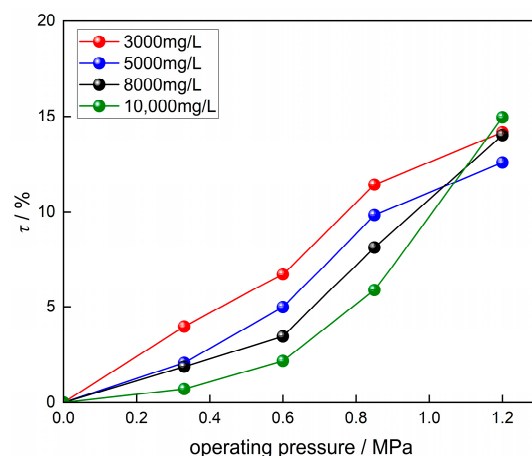

Figure 13. Solute rejection by the ionic membrane at different operating pressures.

In the initial stage of increasing pressure, the rate of change in the solute rejection rate is relatively slow, while in the later stage, the rate of change increases. At a low salt concentration of 3000 mg/L, as the pressure increases, the minimum and maximum ratio of the solute removal rate change are 3.96% (0.33 MPa) and 14.17% (1.2 MPa), respectively. At a salt concentration of 5000 mg/L, the minimum and maximum ratio of the solute rejection rate change are 2.07% (0.33 MPa) and 12.59% (1.2 MPa), respectively. At a salt concentration of 8000 mg/L, the minimum and maximum ratio of the solute rejection rate change are 1.87% (0.33 MPa) and 14.02% (1.2 MPa), respectively. At a higher salt concentration of 10,000 mg/L, the minimum and maximum ratio of the solute rejection rate change are 0.7% (0.33 MPa) and 14.95% (1.2 MPa), respectively. Due to the high pressure approaching the pressure of the feed water salt concentration, the RO membrane produces a large amount of water, resulting in a rapid increase in the concentration of the solution in the equipment, increasing the impact of the concentration change on the solute rejection rate. Therefore, under a higher level of pressure, the rate of change in the solute rejection rate of the ion-exchange membrane increases faster.

Figure 14 depicts the variation in the ion-exchange membrane current efficiency with pressure related to a voltage of 15 V. The operating pressure of 0 MPa represents the current efficiency value for the single-field experiment. From the graph, it can be observed that pressure has an impact on the current efficiency, which is generally higher than that of the single-field case. The formula for current efficiency indicates that it is positively correlated with the solute rejection rate and negatively correlated with the current.
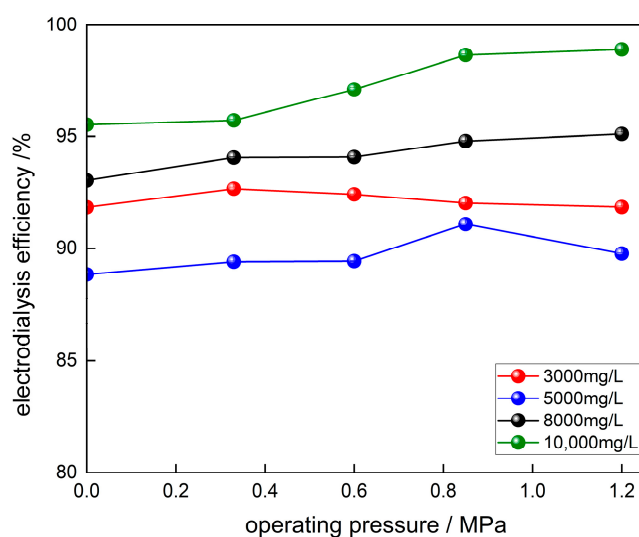

Figure 14. The current efficiency of ionic membranes at different operating pressures.

Under low salinity conditions (3000 mg/L, 5000 mg/L), the current efficiency demonstrates an increasing trend, followed by a decrease, with maximum values of 92.66% and 91.08%, respectively. This is due to the increasing solute rejection rate and permeate flux of the RO membrane with increasing pressure in low salinity conditions. Below 0.85 MPa, the concentration effect of RO has a minimal impact on the current increase, resulting in a relatively constant current and an increasing trend in the current efficiency. However, as the pressure continues to rise, the solute rejection rate of the ion-exchange membrane increases, leading to an increase in the current and, subsequently, a decrease in the current efficiency.

For higher salinity conditions (8000 mg/L, 10,000 mg/L), the current efficiency exhibits an increasing trend, but the magnitude of the increase is not significant, with maximum values of 95.10% and 98.92%, respectively. This can be attributed to the relatively low solute rejection rate and permeate flux during RO of below 0.85 MPa, resulting in minimal changes in the current. Nevertheless, the convective mass transfer of the ion-exchange membrane intensifies due to the increased turbulence, leading to a gradual increase in the

current efficiency. Beyond 0.85 MPa, the concentration effect of RO becomes prominent, causing an increase in the current and a stable region in regard to the current efficiency.

3.4. SEC Analysis

The main energy consumed by the EDRO system comes from the high-pressure pump and the DC power supply. The high-pressure pump provides the energy for the RO process, while the DC power supply provides the energy for the ion-exchange membrane. The specific energy consumption (*SEC*) formula for RO is as follows, assuming that the pump efficiency is 100%:

$$SEC = \frac{W_t}{Q_p} \tag{6}$$

$$W_t = P \times t \tag{7}$$

where *SEC* (kW·h/m^3) represents the amount of electricity consumed per unit volume of water produced in a unit of time; W_t (kW·h) represents the work conducted by the pump in the processing time t; P (kW) represents the power of the pump; t (h) represents the operating time of the pump; Q_p (m^3) represents the total amount of water that passes through RO in time t.

The formula for calculating the SEC_d of ion-exchange membranes in the presence of an electric field only is as follows:

$$SEC_d = \frac{UIt \times 10^{-3}}{Q_0} \tag{8}$$

where U (V) is the operating voltage, I (A) is the operating current, and Q_0 is the total amount of solution treated; here, it is 4.5 L.

To ensure the comparability of energy consumption in ion membranes, it is necessary to compare the electrical energy consumption at the same solute rejection rate. The main difference between the coupled system and the single electric field lies in the higher solute rejection rate in the coupled system within the same reaction time. To ensure the same solute rejection rate, the reaction time in the coupled system is correspondingly reduced. Therefore, when calculating the *SEC*, a coefficient is multiplied to estimate the reaction time of the coupled system, and the energy consumption is calculated based on that. The formula for the SEC_o in the coupled system is as follows:

$$SEC_O = \varphi \times SEC_d \tag{9}$$

$$\varphi = \frac{R_d}{R_o} \tag{10}$$

where R_d is the solute rejection rate of the ionic membrane when only the electric field is present, and R_o is the solute rejection rate of the ionic membrane when both the electric and pressure fields are present.

The results were analyzed using the specific energy consumption reduction rate, calculated using the following formula:

$$\varnothing = \left(1 - \frac{SEC_o}{SEC_d}\right) \times 100\% \tag{11}$$

From Figure 15a, it is evident that the *SEC* reduction rate of the RO membrane gradually increases with an increase in voltage. For a feed concentration of 5000 mg/L, the *SEC* reduction rate improves from 4.8% to 9.5%. Similarly, for a feed concentration of 10,000 mg/L, the *SEC* reduction rate increases from 13.3% to 19.2%. This demonstrates that, under the same feed flow rate, increasing the electric field can effectively reduce the *SEC* during RO. The reason behind this phenomenon is that an increased electric field enhances the permeate flux in RO. As per the calculation formula for the *SEC* (Equation (6)),

an increased permeate flux leads to a higher amount of water production, resulting in a reduced *SEC*.
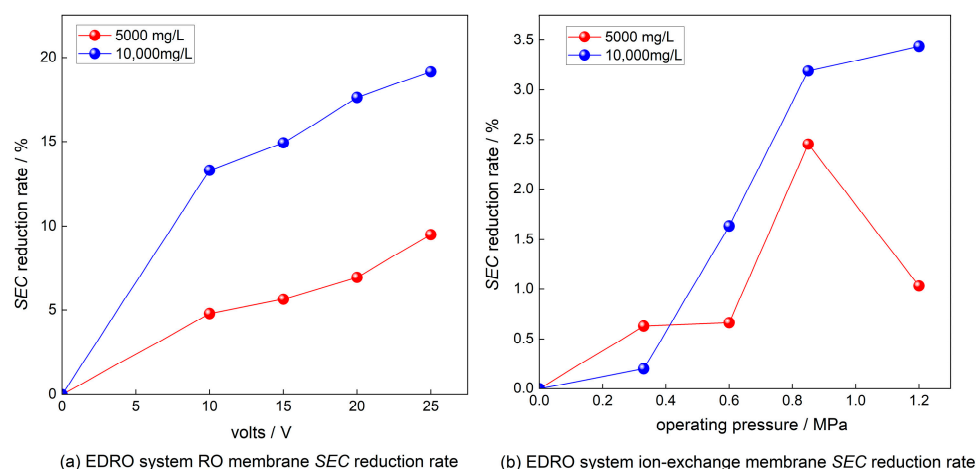

(a) EDRO system RO membrane *SEC* reduction rate   (b) EDRO system ion-exchange membrane *SEC* reduction rate

Figure 15. *SEC* analysis. (**a**) *SEC* reduction rate during RO in EDRO system, (**b**) *SEC* reduction rate of the ion-exchange membrane in EDRO system.

From Figure 15b, it can be observed that for the ion-exchange membrane, the *SEC* reduction rate initially increases and then decreases with an increase in pressure, for a feed concentration of 5000 mg/L. The maximum *SEC* reduction rate is 2.5%. The reason behind this behavior is that as the pressure increases to a certain extent, the RO concentration effect becomes more prominent, leading to an increase in the ion concentration, a decrease in the electrical resistance, and a higher current amplification rate. According to the calculation formula for the *SEC* of ion-exchange membranes, the *SEC* is increased with an increase in the current, but is inversely proportional to the solute retention rate. Since the current increases, the solute rejection rate of the ion-exchange membrane increases more significantly than the increase in current, resulting in a decrease in the *SEC*. For a feed concentration of 10,000 mg/L, the *SEC* reduction rate for the ion-exchange membrane initially increases at a higher rate, with an increase in pressure. However, when the pressure exceeds 0.85 MPa, the rate of increase slows down, and the maximum *SEC* reduction rate is 3.4%. The reason behind this trend is that at lower pressures, the RO concentration effect is less pronounced, resulting in a smaller rate of increase in the current. However, when the pressure surpasses 0.85 MPa, which is the design pressure for the RO membrane under this concentration, the concentration effect becomes more significant, leading to a higher rate of increase in the current and an increasing rate of solute rejection by the ion-exchange membrane. This eventually results in a slowing down of the rate of increase in the *SEC* reduction.

4. Conclusions

This study introduces the development of a novel desalination device called the coupled EDRO. The research showcases the device's operational feasibility and demonstrates the mutual enhancements to the desalination performance by coupling ion-exchange membranes with RO membranes. The study findings indicate that the concentration effect of RO improves the solute rejection rate of ED. Simultaneously, the function of ion-exchange membranes creates a relatively dilute compartment for RO, enhancing its permeate flux under the influence of electric and pressure fields.

When the device is in a coupled state, an increase in voltage leads to a proportional increase in the permeate flux of RO, particularly at higher salt concentrations of 8000 and 10,000 mg/L. The maximum relative permeate flux changes are 21.2% and 23.7%, respectively. There is a strong correlation between voltage and permeate flux, with R^2

values above 0.9. However, voltage has a less significant impact on the solute rejection rate of RO.

In the coupled state, applying pressure enhances the degree of turbulence of the solution, thereby increasing the convective mass transfer rate and promoting solute rejection through ion-exchange membranes. The relative solute rejection rate changes with a pressure increase for salt concentrations of 3000, 5000, 8000, and 10,000 mg/L are 14.17%, 12.59%, 14.02%, and 14.95%, respectively.

The *SEC* analysis reveals that both RO and ED consume less energy compared to when they operate individually.

In conclusion, the coupling of ion-exchange membranes with RO membranes in a single device offers space-saving benefits and improved desalination performance. Nonetheless, this study has certain limitations, and further research is required to investigate ion migration behavior within the coupled EDRO device, as well as the desalination performance of the EDRO device in the presence of other pollutants. Such research will provide a solid theoretical basis for the development of the device. Furthermore, the utilization of more suitable RO membranes, such as hollow-fiber membranes, should be considered to enhance the membrane area and improve the RO performance.

References

1. Salehi, M. Global Water Shortage and Potable Water Safety; Today's Concern and Tomorrow's Crisis. *Environ. Int.* **2022**, *158*, 106936. [CrossRef] [PubMed]
2. Koop, S.H.A.; Grison, C.; Eisenreich, S.J.; Hofman, J.; Van Leeuwen, K. Integrated Water Resources Management in Cities in the World: Global Solutions. *Sustain. Cities Soc.* **2022**, *86*, 104137. [CrossRef]
3. Magri, A.; Berezowska-Azzag, E. New Tool for Assessing Urban Water Carrying Capacity (WCC) in the Planning of Development Programs in the Region of Oran, Algeria. *Sustain. Cities Soc.* **2019**, *48*, 101316. [CrossRef]
4. Zhang, J.; Zhang, C.; Shi, W.; Fu, Y. Quantitative Evaluation and Optimized Utilization of Water Resources-Water Environment Carrying Capacity Based on Nature-Based Solutions. *J. Hydrol.* **2019**, *568*, 96–107. [CrossRef]
5. Al-Amshawee, S.; Yunus, M.Y.B.M.; Azoddein, A.A.M.; Hassell, D.G.; Dakhil, I.H.; Hasan, H.A. Electrodialysis Desalination for Water and Wastewater: A Review. *Chem. Eng. J.* **2020**, *380*, 122231. [CrossRef]
6. Feria-Díaz, J.J.; Correa-Mahecha, F.; López-Méndez, M.C.; Rodríguez-Miranda, J.P.; Barrera-Rojas, J. Recent Desalination Technologies by Hybridization and Integration with Reverse Osmosis: A Review. *Water* **2021**, *13*, 1369. [CrossRef]
7. Zubair, M.M.; Saleem, H.; Zaidi, S.J. Recent Progress in Reverse Osmosis Modeling: An Overview. *Desalination* **2023**, *564*, 116705. [CrossRef]
8. Moriyama, N.; Nagasawa, H.; Kanezashi, M.; Tsuru, T. Water Permeation in Gas and Liquid Phases through Organosilica Membranes: A Unified Theory of Reverse Osmosis, Pervaporation, and Vapor Permeation. *Chem. Eng. Sci.* **2022**, *263*, 118083. [CrossRef]
9. Shah, K.M.; Billinge, I.H.; Chen, X.; Fan, H.; Huang, Y.; Winton, R.K.; Yip, N.Y. Drivers, Challenges, and Emerging Technologies for Desalination of High-Salinity Brines: A Critical Review. *Desalination* **2022**, *538*, 115827. [CrossRef]
10. Bai, W.; Samineni, L.; Chirontoni, P.; Krupa, I.; Kasak, P.; Popelka, A.; Saleh, N.B.; Kumar, M. Quantifying and Reducing Concentration Polarization in Reverse Osmosis Systems. *Desalination* **2023**, *554*, 116480. [CrossRef]

11. Lee, S.; Choi, J.; Park, Y.-G.; Shon, H.; Ahn, C.H.; Kim, S.-H. Hybrid Desalination Processes for Beneficial Use of Reverse Osmosis Brine: Current Status and Future Prospects. *Desalination* **2019**, *454*, 104–111. [CrossRef]

12. Wang, Z.; Zhang, Y.; Wang, T.; Zhang, B.; Ma, H. Design and Energy Consumption Analysis of Small Reverse Osmosis Seawater Desalination Equipment. *Energies* **2021**, *14*, 2275. [CrossRef]

13. Shahi, V.K.; Makwana, B.S.; Thampy, S.K.; Rangarajan, R. A Novel Electrodialyzer for the Production of Demineralized Water by Electrodialysis. *Desalination* **2003**, *151*, 33–42. [CrossRef]

14. Tan, N.P.B.; Ucab, P.M.L.; Dadol, G.C.; Jabile, L.M.; Talili, I.N.; Cabaraban, M.T.I. A Review of Desalination Technologies and Its Impact in the Philippines. *Desalination* **2022**, *534*, 115805. [CrossRef]

15. Sirivedhin, T.; McCue, J.; Dallbauman, L. Reclaiming Produced Water for Beneficial Use: Salt Removal by Electrodialysis. *J. Membr. Sci.* **2004**, *243*, 335–343. [CrossRef]

16. Patel, S.K.; Biesheuvel, P.M.; Elimelech, M. Energy Consumption of Brackish Water Desalination: Identifying the Sweet Spots for Electrodialysis and Reverse Osmosis. *ACS EST Eng.* **2021**, *1*, 851–864. [CrossRef]

17. Shestakov, K.V.; Lazarev, S.I.; Selivanov, Y.T.; Khokhlov, P.A.; Lomakina, O.V. Mathematical Description and Method of Calculating the Technological Parameters of an Electrodialysis Apparatus for Chemical Industrial Wastewater Treatment. *Chem. Petrol. Eng.* **2020**, *56*, 53–58. [CrossRef]

18. Shi, J.; Gong, L.; Zhang, T.; Sun, S. Study of the Seawater Desalination Performance by Electrodialysis. *Membranes* **2022**, *12*, 767. [CrossRef]

19. Voutetaki, A.; Plakas, K.V.; Papadopoulos, A.I.; Bollas, D.; Parcharidis, S.; Seferlis, P. Pilot-Scale Separation of Lead and Sulfate Ions from Aqueous Solutions Using Electrodialysis: Application and Parameter Optimization for the Battery Industry. *J. Clean. Prod.* **2023**, *410*, 137200. [CrossRef]

20. Mir, N.; Bicer, Y. Integration of Electrodialysis with Renewable Energy Sources for Sustainable Freshwater Production: A Review. *J. Environ. Manag.* **2021**, *289*, 112496. [CrossRef]

21. Elsaid, K.; Sayed, E.T.; Abdelkareem, M.A.; Mahmoud, M.S.; Ramadan, M.; Olabi, A.G. Environmental Impact of Emerging Desalination Technologies: A Preliminary Evaluation. *J. Environ. Chem. Eng.* **2020**, *8*, 104099. [CrossRef]

22. La Cerva, M.; Gurreri, L.; Tedesco, M.; Cipollina, A.; Ciofalo, M.; Tamburini, A.; Micale, G. Determination of Limiting Current Density and Current Efficiency in Electrodialysis Units. *Desalination* **2018**, *445*, 138–148. [CrossRef]

23. Generous, M.M.; Qasem, N.A.A.; Zubair, S.M. An Innovative Hybridization of Electrodialysis with Reverse Osmosis for Brackish Water Desalination. *Energy Convers. Manag.* **2021**, *245*, 114589. [CrossRef]

24. Zhang, X.; Zhang, C.; Meng, F.; Wang, C.; Ren, P.; Zou, Q.; Luan, J. Near-Zero Liquid Discharge of Desulfurization Wastewater by Electrodialysis-Reverse Osmosis Hybrid System. *J. Water Process Eng.* **2021**, *40*, 101962. [CrossRef]

25. Nayar, K.G.; Fernandes, J.; McGovern, R.K.; Dominguez, K.P.; McCance, A.; Al-Anzi, B.S.; Lienhard, J.H. Cost and Energy Requirements of Hybrid RO and ED Brine Concentration Systems for Salt Production. *Desalination* **2019**, *456*, 97–120. [CrossRef]

26. Walker, W.S.; Kim, Y.; Lawler, D.F. Treatment of Model Inland Brackish Groundwater Reverse Osmosis Concentrate with Electrodialysis—Part I: Sensitivity to Superficial Velocity. *Desalination* **2014**, *344*, 152–162. [CrossRef]

27. Gurreri, L.; La Cerva, M.; Moreno, J.; Goossens, B.; Trunz, A.; Tamburini, A. Coupling of electromembrane processes with reverse osmosis for seawater desalination: Pilot plant demonstration and testing. *Desalination* **2022**, *526*, 115541. [CrossRef]

28. Reig, M.; Casas, S.; Aladjem, C.; Valderrama, C.; Gibert, O.; Valero, F.; Centeno, C.M.; Larrotcha, E.; Cortina, J.L. Concentration of NaCl from Seawater Reverse Osmosis Brines for the Chlor-Alkali Industry by Electrodialysis. *Desalination* **2014**, *342*, 107–117. [CrossRef]

29. Zhang, Y.; Ghyselbrecht, K.; Meesschaert, B.; Pinoy, L.; Van Der Bruggen, B. Electrodialysis on RO Concentrate to Improve Water Recovery in Wastewater Reclamation. *J. Membr. Sci.* **2011**, *378*, 101–110. [CrossRef]

30. Munshi, F.M.; Hwang, J.-H.; Park, J.; Sadmani, A.; Khan, M.A.; Jeon, B.-H.; Lee, W.H. Electric Field Forward Osmosis (EFFO) Fouling Mitigation in Algae Harvesting. *Sep. Purif. Technol.* **2023**, *327*, 124868. [CrossRef]

31. Ji, Y.; Choi, Y.J.; Fang, Y.; Pham, H.S.; Nou, A.T.; Lee, L.S.; Niu, J.; Warsinger, D.M. Electric Field-Assisted Nanofiltration for PFOA Removal with Exceptional Flux, Selectivity, and Destruction. *Environ. Sci. Technol.* **2023**, *57*, 18519–18528. [CrossRef] [PubMed]

32. Cao, S.; Wang, Y.; Zhang, Y.; Wang, G.; Su, T. Inhibition of Membrane Fouling by Frequency Agility Electric Field in Desalination. *J. Environ. Chem. Eng.* **2023**, *11*, 110740. [CrossRef]

33. Zoungrana, A.; Çakmakci, M. Optimization of the Reverse Electrodialysis Power Output through the Ratio of the Feed Solutions Salinity. *IET Renew. Power Gen.* **2021**, *15*, 769–777. [CrossRef]

34. Sadrzadeh, M.; Mohammadi, T. Sea Water Desalination Using Electrodialysis. *Desalination* **2008**, *221*, 440–447. [CrossRef]

35. Banasiak, L.J.; Kruttschnitt, T.W.; Schäfer, A.I. Desalination Using Electrodialysis as a Function of Voltage and Salt Concentration. *Desalination* **2007**, *205*, 38–46. [CrossRef]

36. Ansari, M.; Al- Obaidi, M.A.; Hadadian, Z.; Moradi, M.; Haghighi, A.; Mujtaba, I.M. Performance Evaluation of a Brackish Water Reverse Osmosis Pilot-Plant Desalination Process under Different Operating Conditions: Experimental Study. *Clean. Eng. Technol.* **2021**, *4*, 100134. [CrossRef]

37. Sitterley, K.A.; Cath, T.J.; Jenne, D.S.; Yu, Y.-H.; Cath, T.Y. Performance of Reverse Osmosis Membrane with Large Feed Pressure Fluctuations from a Wave-Driven Desalination System. *Desalination* **2022**, *527*, 115546. [CrossRef]

38. Al-Obaidi, M.A.; Alsarayreh, A.A.; Bdour, A.; Jassam, S.H.; Rashid, F.L.; Mujtaba, I.M. Simulation and Optimisation of a Medium Scale Reverse Osmosis Brackish Water Desalination System under Variable Feed Quality: Energy Saving and Maintenance Opportunity. *Desalination* **2023**, *565*, 116831. [CrossRef]

39. Salahudeen, N. Process Simulation of Modelled Reverse Osmosis for Desalination of Seawater. *Water Pract. Technol.* **2022**, *17*, 175–190. [CrossRef]

40. Du, J.R.; Du, W.; Feng, X.; Zhang, Y.; Wu, Y. Membrane Distillation Enhanced by an Asymmetric Electric Field. *AIChE J.* **2014**, *60*, 2307–2313. [CrossRef]

41. Giri, A.K.; Teixeira, F.; Cordeiro, M.N.D.S. Salt Separation from Water Using Graphene Oxide Nanochannels: A Molecular Dynamics Simulation Study. *Desalination* **2019**, *460*, 1–14. [CrossRef]

42. Phan, L.X.; Lynch, C.I.; Crain, J.; Sansom, M.S.P.; Tucker, S.J. Influence of Effective Polarization on Ion and Water Interactions within a Biomimetic Nanopore. *Biophys. J.* **2022**, *121*, 2014–2026. [CrossRef] [PubMed]